Fabrication and Study of the Effect of Mn-Substituted Ba-Zn Nanoferrites on the Enrichment of Structural Properties

A. H. AL-Hammadi [1], Azmi A. M. Othman[1,3,*], Sadiq. H. Khoreem[1,2]

[1] Physics Department, Faculty of Science, Sana'a University, Sana'a, Yemen.
[2] Department of Optometry and Vision Science, Faculty of Medical Sciences, Al-Razi University, Sana'a, Yemen.
[3] Yemen Standardization, Metrology, and Quality Control Organization (YSMO).
*Corresponding author: azmihameed@yahoo.com.

ABSTRACT: In this study, we investigated the impact of manganese doping on the structural properties of barium-zinc ferrites (BZF-NPs) synthesized using the traditional ceramic method. X-ray diffraction (XRD) was used to analyze the structural characteristics of the BZF-NPs, including the structure phases, crystallite size, and lattice parameter. Also calculated various physical properties, such as bulk density, X-ray density, porosity, and specific surface area. The samples XRD analysis revealed that the lattice parameters of the hexagonal M-type structure of the BZF-NPs decreased as the concentration of Mn^{2+} ions increased. Also observed a decrease in the average crystallite size of the samples from 52 to 42 nm with increasing Mn^{2+} concentration. The ratio of the c/a parameters indicated the formation of a magnetoplumbite structure. Moreover, we found that both X-ray density and bulk density increased with increasing Mn^{2+} concentration. This behavior can be attributed to the difference in ionic radius between donor Mn^{2+} ions and host Fe^{3+} and Zn^{2+} ions. However, it was observed that porosity increased with increasing Mn^{2+} concentration, in contrast to the behavior of bulk density. Furthermore, it was observed that as the crystallite size increased, the surface area decreased. This trend can be attributed to the fact that larger crystallite sizes have fewer surface atoms. Finally, it is noted that the bond length for both tetrahedral and octahedral structures decreased with increasing Mn^{2+} ion concentration.Overall, these results provide insights into the impact of Mn^{2+} ion doping on the structural and physical properties of BZF-NPs, and highlight the potential applications of these materials in various fields.

CONTENTS
1. Introduction
2. Materials and Methods
3. Results and Discussion
4. Conclusion
5. References

1. Introduction

Nanotechnology research is a rapidly expanding field that is attracting increasing attention due to its unique properties and diverse applications in fields such as engineering and medicine. Nanoparticles at the nanoscale level are being studied to enhance their physical, optical, electronic, and compositional properties, for use in various applications including biomedicine, electrocatalysts, biosensors, magnetic refrigeration, water decontamination, and electronic equipment [1–5]. Ferroelectric materials have drawn increased attention from scientists lately. Since their discovery, many kinds of ferrite nanoparticles, sometimes known as ferrite nanoparticles, have traveled a great distance [5,6]. M-type for its scientific uses in ferromagnetic materials and promising applications in high-performance magnetic data storage devices. M-type $BaFe_{12}O_{19}$ with rare earth doping elements such as Neodymium (Nd) and Samarium. Additionally, barium hexaferrite is preferred for microwave frequencies because of its extensive nanocrystals [7]. Ferrites' structural and electromagnetic properties can be changed by synthesizing them and doping them with various rare metals and metallic ions in hexagonal arrangements [8]. Ferrites' essential properties, including permittivity, dielectric losses, and conductivity, are controlled by their composition, processing technique, and type of metallic ions deposited into them. [9]. Gilani, et ale, cerium (Ce^{3+}), a rare-earth metal, and barium ferrite nanoparticles with micro-structural activity ($BaCe_xFe_{12-x}O_{19}$). Elemental substitutions can improve the electromagnetic and dielectric properties of nanoparticles with ferric (Fe^{3+}) sites. Barium ferrite nanoparticles with cerium (Ce^{3+}) doping were shown to have much better excellent adsorption qualities, indicating that ($BaCe_xFe_{12-x}O_{19}$) can be

employed in electromagnetic techniques, high memory sticks, and electronic components. [10]. The sol-gel method is used to create the barium ferrite nanoparticles ($BaZn_xFe_{12-x}O_{19}$) with zinc (Zn) as a substituent. $BaFe_{12-x}Mn_xO_{19}$, where x was 0.5, 1.0, 1.5, and 2.0, was examined as barium modified with a modest quantity of Mn. According to the findings, ac conductivity increased as Mn quantity grew. While the lattice parameter fell. This entails a reduction in lattice volume[11]. The microstructure, ferromagnetic, and electromagnetic characteristics of BaFeO nanostructures have been extensively studied with variations in Pe, Cr, Zn, Ce, and doping concentration, but there is a need for more research to understand their optical properties. This work includes investigations impacts of Mn doping on microstructure behavior for barium hexaferrite with the general formula $Ba\ Zn_{1+x}\ Mn_x\ Fe_{12-2x}\ O_{19}$ (x = 0.4, 0.8, 1.2, 1.6, and 2).

2. Materials And Methods

A composition sample of the $BaZn_{1+x}Mn_xFe_{12-2x}O_{19}$ M-type ferrite system (where x = 0.0, 0.4, 0.8, 1.2, 1.6, and 2) has been synthesized via the usual ceramics technique as explained earlier [12,13]. In this study, XRD was used to evaluate the crystal structure and phase composition of the $BaZn_{1+x}Mn_xFe_{12-2x}O_{19}$ ferrite system. The EDX-720 diffractometer used in this study is a model produced by Shimadzu and operates by directing X-rays at a sample and measuring the intensity of the diffracted X-rays as a function of the scattering angle (2θ). The range of 2θ values used in this study was 3-75 degrees, and the scanning rate was 0.02 min^{-1}. The XRD patterns collected from the samples can be used to determine the lattice parameters, crystal structure, and phase composition of the synthesized materials

3. Results And Discussion

3.1 XRD results.

The phase types of nanocrystals in BaZnMnFeO-NPs were characterized using an XRD pattern obtained from BaZnMnFeO-NPs prepared via the traditional ceramic method, as depicted in Figure 1. The XRD spectra show no impurities, indicating the presence of a pure phase for BaZnMnFeO-NPs. A recent study investigated the effects of partially substituting manganese on the crystal size, united cell volume, and lattice characteristics of experimental ferrite nanoparticles. The lattice cell constants *a* and *c* have been calculated through the following expression [13],.
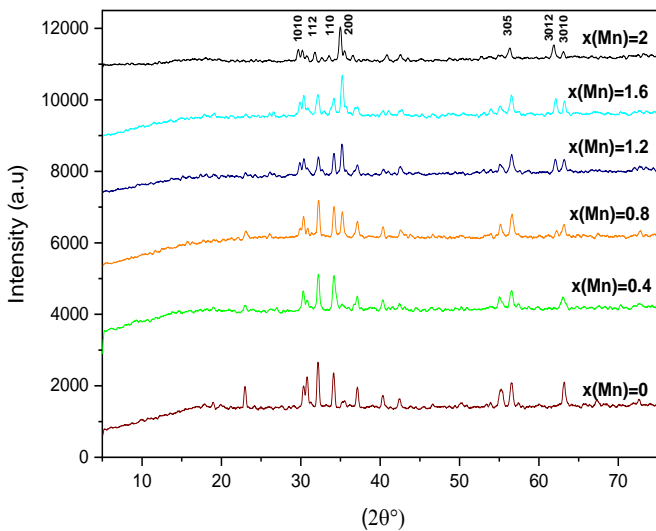
Figure. 1: X-ray diffraction patterns of $BaZn_{1-x}Mn_xFe_{12-x}O_{19}$,(x=0, 0.4, 0,8, 1.2, 1.6, and 2)

$$\frac{1}{d_{hkl}^2} = \frac{4}{3}\frac{h^2+hk+k^2}{a^2} + \frac{L^2}{C^2} \quad (1)$$

Where d is the inter planner distance and h, k and l are the Miller indices of the peaks.

Due to the slight difference in ionic radii, the lattice parameters and unit cell volume for Mn-doped particle magnetite are marginally lower than those for pure $BaZnFe_{12}O_{19}$, and these values decrease with an increase in Mn doping levels as shown in

figure.2. This reduction can be attributed to the lower ionic radii of metal cations and Zn ions (0.64 and 0.74, respectively) compared to Mn^{2+} (0.80). Moreover, as Mn^{2+} ions increase in ferrite, Fe^{3+} ions migrate from the A site to the B site, causing a widening of the lattice and an increase in lattice constant due to the larger ions, Mn^{2+} (0.80 Å), over Fe^{3+} (0.67 Å) and Zn^{2+} (0.74 Å). The c/a value in the experimental specimens, as shown in Fig. 2, falls within this range, indicating that the phenomenon occurs, and the structure forms.
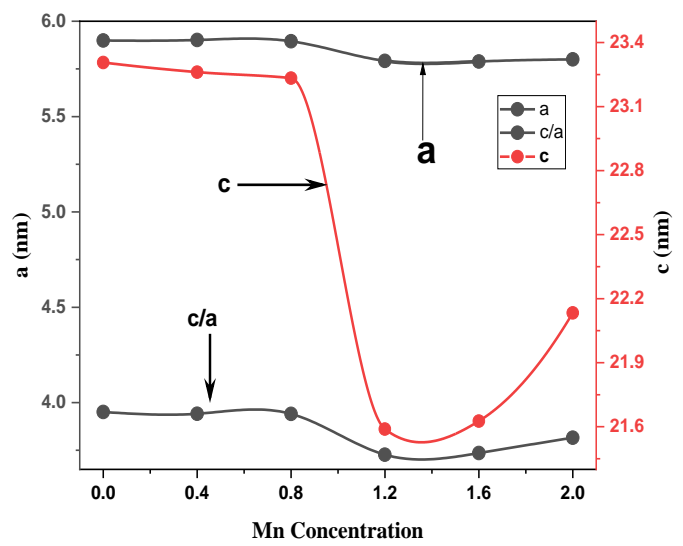
Figure 2. The relation between lattice parameters (a), (b) and ratio (c/a), with Mn^{2+} ions concentration for $BaZn_{1+x}Mn_xFe_{12-2x}O_{19}$.

The volume of the unit cell V is calculated by using the flowing formula {2} [13]:

$$V = 0.866\ a^2c \quad (2)$$

Where α and c are the lattice constants. The cell volume values of manganese doped barium-zinc nano particles ferrites with (x = 0.0, 0.4, 0.8, 1.2, 1.6, and 2.0) is shown in the (figure,3). The unit cell volume varies with different Mn^{2+} ions concentration, while at (x = 1.2) cell volume reaches to minimum value. The cell volume is found to be in a range 627.577 – 702.4033 nm^3.
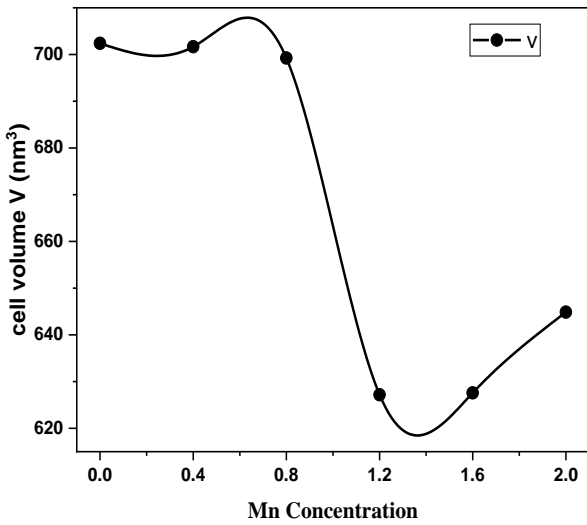
Figure 3. The cell volume with Mn^{2+} ions concentration for $BaZn_{1+x}Mn_xFe_{12-2x}O_{19}$.

The experimental density ρ_B, was determined using the formula(3) :

$$\rho_B = \frac{m}{\pi r^2 h} \qquad (3)$$

As shown in Figure 4, the experimental density increased from 4.5 to 5.5 g/cm^3 with an increase in doping percentage of Mn. This increase in density is attributed to the contrast in atomic radii between the donor ions Mn and the guest ions Zn and Fe. Also, the contrast in atomic radius between the donor ions Mn, as well as the guest ions Zn and Fe, is the reason that caused this rise in experiment density.

The XRD density (ρ_x) of the samples was calculated using the following formula [14]:

$$\rho_x = \frac{ZM}{N_A V} \qquad (4)$$

where Z is the number of formula units, M is the molecular weight, N_A is Avogadro's number, and V is the unit cell volume.

The values of XRD density obtained are shown in Figure 4. The results indicate an increase in XRD density with an increase in Mn perovskite concentration. This increase is influenced by the sample's molecular weight..
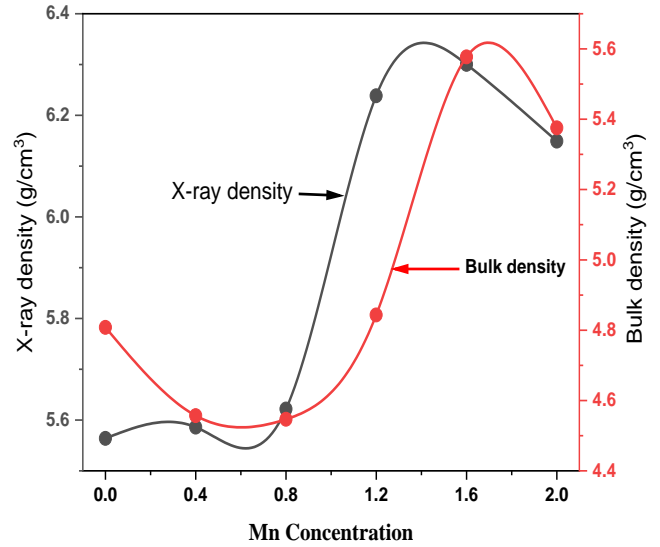
Figure 4. XRD density, and bulk density with Mn concentration for $BaZn_{1+x}Mn_xFe_{12-2x}O_{19}$.

3.2 Crystalline Size

The average grain size (D) for the samples was calculated from the x-ray diffraction pattern via Scherrer's relation [15]:

D = 0.9λ/βcosθ.   (5)

The prepared samples had an average grain size ranging between 53-42 nm, as illustrated in Fig. 5. Compounds with average crystalline sizes below 50 nm are commonly considered to have a high signal-to-noise ratio for high-density recording medium [16]. Dislocation density of the synthesis nanoparticles ferrites is calculated by using the flowing formula:

$$\boldsymbol{\delta} = \mathbf{1} / \boldsymbol{D^2} \qquad (6)$$

The crystallite size is denoted by D. Dislocation density also has inverse relation with crystallite size as shown in figure,5. The density of dislocations is found to be between 3.69 – 5.17 x 10^{14} (lines / m^2). It is observed that first it increased then decreases to lower value at (x=0.8) than rises in proportion to the substituent concentration. At (x = 2.0), the maximal value of dislocation density is found, which shows the crystalline size D is minimum at that point (D=43.97nm).
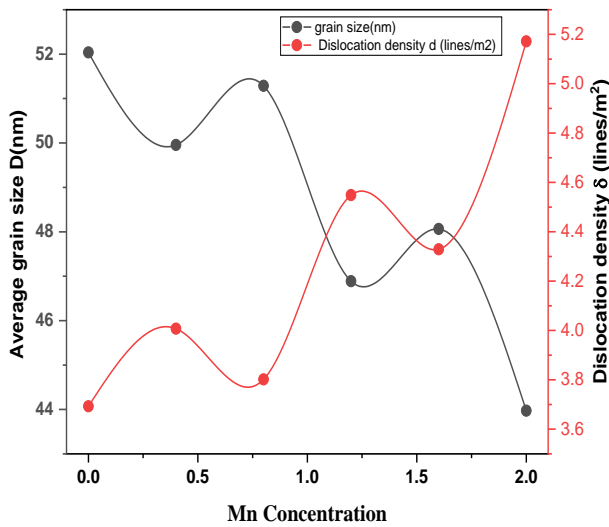
Figure 5. The relation average crystallite size, and dislocation with Mn concentration for BaZn$_{1+x}$Mn$_x$Fe$_{12-2x}$O$_{19}$.

3.3. Relative Porosity and Specific surface area.

Relative porosity (%P) of the synthesized samples was determined using the x-ray density and experimental density with the following equation:

$$\%P = \left(\frac{\rho_x - \rho_B}{\rho_x}\right) \times 100 \qquad (7)$$

Relative porosity is a critical factor in determining the physical and chemical properties of the samples. The results show that as the Mn doping concentration increased, porosity increased up to 1.2, after which it decreased, as shown in figure,6. This behavior is observed due to Mn is larger ionic radius than Zn and Fe, which leads to the production of fewer cations and more oxygen-containing functional groups, ultimately resulting in decreased porosity,[17]. It is also noteworthy that the porosity behavior is opposite to the bulk density, and the structure with x = 1.6 has

the smallest porosity and the largest bulk density [18].

The following equation is used to calculate the specific surface area (S) of the synthesized components [19]:

$$S = \frac{6000}{D\rho_x} \qquad (8)$$

Figure 6, illustrates the changes in the specific surface area (S) with respect to the concentration of Mn ions. At x = 0.4, the surface area remains consistently high. The increase in surface area may be due to the reduction in crystallite size. However, as the concentration of Mn ions increases, the surface area decreases, possibly due to particle size growth. Fig. 2 also shows that at Mn = 2, there is a smaller particle size and a larger surface area. This suggests that as the amount of particle surface increases, the average crystalline size decreases, leading to a larger surface area. It is also important to note that as the concentration of nanoparticles increases, the surface area decreases.
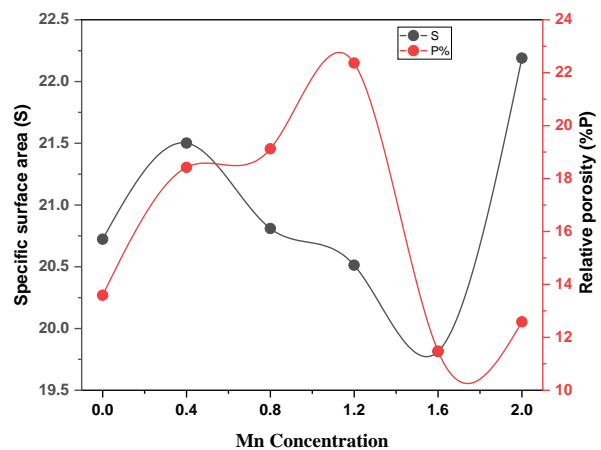
Figure 6. The relation between Relative porosity (%P) and specific surface area (S), with Mn^{2+} ions concentration for BaZn$_{1+x}$Mn$_x$Fe$_{12-2x}$O$_{19}$.

Additionally, using the following equations, the distances between magnetic ions and hopping distances in tetrahedral sites (L$_A$) and

octahedral sites (L_B) were calculated [19,20,21].

$$L_A = 0.25a\sqrt{3} \qquad (9)$$
$$L_B = 0.25a\sqrt{2} \qquad (10)$$

Figure 7, illustrates the values of L_A and L_B and the correlation between the hopping distances in sites with octahedral and tetrahedral containing Mn. As the concentration of Mn^{2+} ions increases, the hopping length decreases. This behavior may be attributed to the variation in the lattice constant with the Mn content. In other words, the decrease in space between magnetic ions is a result of the increase in magnetic ion Mn concentration and the decrease in non-magnetic ions Zn. This is likely due to the fact that both Zn^{2+} ions and Fe^{3+} ions have smaller radii (0.74 and 0.64, respectively) than Mn^{2+} ions (0.80). Therefore, as the concentration of Mn ions increases, the distance between magnetic ions decreases.
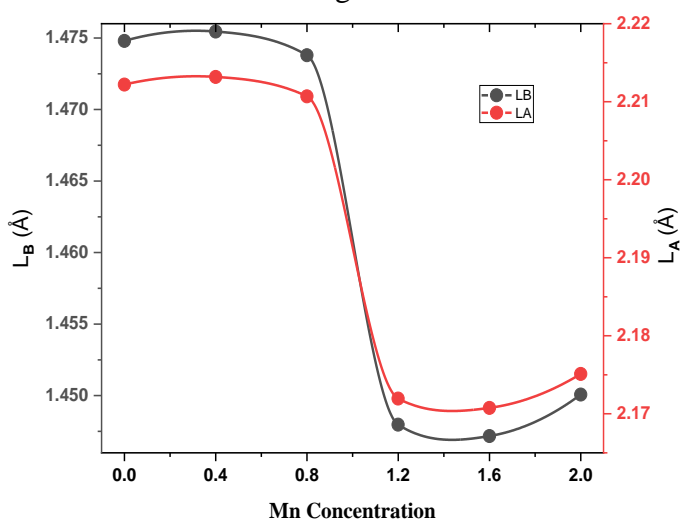
Figure 7. Hoping lengths at the octahedral (LA) and tetrahedral (LB) locations.

4. Conclusion

The BaZnMnFeO-NPs have been prepared successfully using ceramic methods. The X-ray diffraction pattern results indicated a single-phase structure. The average crystallite size was to decrease and reached the minimum value at the Mn^{2+} ions concentration increased to 2.0. The ratio value c/a parameters of the hexagonal M-type structure implied that the magnetoplumbite structure was formed. The physical properties such as bulk density, X-ray density, porosity, and surface area were also calculated. X-ray density and bulk density both raises as manganese concentration in samples increases. The difference in ionic radius between donor Mn^{2+}, host Fe^{3+}, and Zn^{2+} ions causes this behavior. At the same time, porosity has the same behavior with Mn concentration as X-ray density. Porosity increased as opposed to bulk density behavior. The surface area becomes smaller when the crystallite size becomes larger, these will become the number of surface atoms and the smaller will be the surface area. The bond length for tetrahedral and octahedral will decrease as the Mn^{2+} ion concentration increases.

5. References

[1] Shah, S. S., Shaikh, M. N., Khan, M. Y., Alfasane, M. A., Rahman, M. M., & Aziz, M. A. (2021). Present status and future prospects of jute in nanotechnology: A review. *The Chemical Record*, *21*(7), 1631-1665. https://doi.10.1007/978-0-387-71619-0.

[2] Chen, Mazari, S. A., Ali, E., Abro, R., Khan, F. S. A., Ahmed, I., Ahmed, M., ... & Shah, A. (2021). Nanomaterials: Applications, waste-handling, environmental toxicities, and future challenges–A review. *Journal of Environmental Chemical Engineering*, *9*(2), 105028. https://www.sciencedirect.com/science/article/pii/S2213343721000063.

[3] Ghaffarkhah, A., Hosseini, E., Kamkar, M., Sehat, A. A., Dordanihaghighi, S., Allahbakhsh, A., ... & Arjmand, M. (2022). Synthesis, applications, and prospects of graphene quantum dots: A comprehensive review.*Small*,*18*(2),2102683. https://onlinelibrary.wiley.com/doi/abs/10.1002/smll.202102683

[4] Chandrasekaran, S., Bowen, C., Zhang, P., Li, Z., Yuan, Q., Ren, X., & Deng, L. (2018). Spinel photocatalysts for environmental remediation, hydrogen generation, CO 2 reduction and photoelectrochemical water splitting. *Journal of Materials ChemistryA*,*6*(24),11078-11104.

https://pubs.rsc.org/en/content/articlehtml/2018/ta/c8ta03669a

[5] Jabbar, R.; Sabeeh, S.H.; Hameed, A.M. Structural, Dielectric and Magnetic Properties of Mn^{+2} Doped Cobalt Ferrite Nanoparticles. *Journal of Magnetism and Magnetic Materials* **2020**, *494*, 165726, https://doi.10.1016/j.jmmm.2019.165726

[6] Pokropivny, V., Lohmus, R., Hussainova, I., Pokropivny, A., & Vlassov, S. (2007). *Introduction to nanomaterials and nanotechnology* (Vol. 1, p. 138). Ukraine: Tartu UniversityPress.

https://www.researchgate.net/profile/Alex

[7] Hashhash, A., Hassen, A., Baleidy, W. S., & Refai, H. S. (2021). Impact of rare-earth ions on the physical properties of hexaferrites $Ba_{0.5}Sr_{0.5}RE_{0.6}Fe_{11.4}O_{19}$,(RE= La, Yb, Sm, Gd, Er, Eu, and Dy). *Journal of Alloys and Compounds*, *873*,159812. https://doi.10.1016/j.jallcom.2021.159812.

[8] Al-Hammadi, A.H.; Khoreem, S.H. Influence of Zn^{+2} Doping on Dielectric Properties of Ba-Based Nanoferrites. Biointerface Res Appl Chem. 2022, 13, 265, http://dx.doi.10.33263/BRIAC133.256

[9] Almessiere, M.A.; Slimani, Y.; Güngüneş, H.; Demir Korkmaz, A.; Trukhanov, S.V.; Guner, S.; Alahmari, F.; Trukhanov, A.V.; Baykal, A. Correlation between Chemical Composition, Electrical, Magnetic and Microwave Properties in Dy-Substituted Ni-Cu-Zn Ferrites. *Materials Science and Engineering:B***2021**,*270*,115202, https://doi.10.1016/j.mseb.2021.115202.

[10] Gilani, Z.A.; Ahmed, A.; Asghar, H.M.N.; Khalid, M. Doping Effect and Microstructure Behavior of Rare-Earth Element Cerium (Ce^{+3}) in Barium Hexaferrite ($BaCexFe_{12-X}O_{19}$) Nanoparticles. *Journal of Materials and Physical Sciences* **2020**, *1*,58–77, https://doi.10.52131/jmps.2020.0102.0007

[11] Sharma, P.; Rocha, R.A.; de Medeiros, S.N.; Paesano, A.; Hallouche, B. Structural, Mössbauer and Magnetic Studies on Mn-Substituted Barium Hexaferrites Prepared by High Energy Ball Milling. *HyperfineInteract.***2008**,*175*,77–84, http://dx.doi.10.1007/s10751-008-9591-2.

[12] Al-Hammadi, A.H.; Khoreem, S.H. Impact of Zinc Substitution on AC Conductivity Behaviors of Hexagonal Ba-Ni Ferrite Nanoparticle. *Biointerface Res Appl Chem* **2022**,*13*,364, https://doi.org/10.33263/BRIAC134.364

[13] Al-Hammadi, A.H.; Khoreem, S.H. Influence of Manganese Doping on Optical Properties of Barium Ferrites Nanoparticles.**2022**,*13*,369, https://doi.org/10.33263/BRIAC134.369

[14] Massit, A.; El Yacoubi, A.; Kholtei, A.; El Idrissi, B.C. XRD and FTIR Analysis of Magnesium Substituted Tricalcium Calcium Phosphate Using a Wet Precipitation Method. *Biointerface Res Appl Chem* **2020**, *11*,8034–8042, http://dx.doi.10.33263/BRIAC111.80348042.

[15] Ghazanfar, U.; Siddiqi, S.A.; Abbas, G. Structural Analysis of the Mn–Zn Ferrites Using XRD Technique. Materials Science and Engineering: B 2005, 118, 84–86, https://doi.10.1016/j.mseb.2004.12.018

[16] Al-Hammadi, A.H.; Khoreem, S.H. Investigations on Optical and Electrical Conductivity of $Ba/Ni/Zn/Fe_{16}O_{27}$ Ferrite Nanoparticles. *Biointerface Res Appl Chem* **2022**, *13*, 168, http://doi.org/10.33263/BRIAC132.168.

[17] Xavier, S.; Jose, D.; George, S.; Alekha, K.V. Structural and Magnetic Characterization of Transition Metal Substituted Ferrite Nanoparticles.; Kothamangalam, India, **2020**;p.060007,https://aip.scitation.org/doi/abs/10.1063/5.0017047

[18] Zhao, J.; Li, F.; Wei, H.; Ai, H.; Gu, L.; Chen, J.; Zhang, L.; Chi, M.; Zhai, J. Superior Performance of ZnCoOx/Peroxymonosulfate System for Organic Pollutants Removal by Enhancing Singlet Oxygen Generation: The Effect of Oxygen Vacancies. *Chemical Engineering Journal* **2021**, *409*,128150, https://doi.10.1016/j.cej.2020.128150

[19] Khoreem, S.H.Al-Hammadi, A.H.; Synthesis and Unveiling the Effect of Nonmagnetic Zn^{2+} Ions on Enrichment of Structural Properties of Barium-Nickel Ferrites. *Biointerface Res. Appl. Chem., Volume 13, Issue5,2023–15thOctober*, https://doi.org/10.33263/BRIAC135.487

[20] Shitole, J.B.; Keshatti, S.N.; Rathod, S.M.; Jadhav, S.S. Y^{3+} Composition and Particle Size Influenced Magnetic and Dielectric Properties of Nanocrystalline $Ni_{0.5}Cu_{0.5}Y_xFe_{2-X}O_4$ Ferrites. *Ceramics International* **2021**, *47*, 17993–18002, https://doi.10.1016/j.ceramint.2021.03.114

[21] Satalkar, M., & Kane, S. N. (2016, October). On the study of structural properties and cation distribution of Zn0. 75-xNixMg0. 15Cu0. 1Fe2O4 nano ferrite: effect of Ni addition. In *Journal of Physics: Conference Series* (Vol. 755, No. 1, p. 012050). IOP Publishing., https://iopscience.iop.org/article/10.1088/1742-6596/755/1/012050.